Journal of Power Sources 241 (2013) 388–395

Contents lists available at SciVerse ScienceDirect

Journal of Power Sources

journal homepage: www.elsevier.com/locate/jpowsour

Fabrication of graphene oxide/polypyrrole nanowire composite for high performance supercapacitor electrodes

Jing Li, Huaqing Xie*, Yang Li

School of Urban Development and Environmental Engineering, Shanghai Second Polytechnic University, Shanghai 201209, PR China

HIGHLIGHTS

- Graphene oxide/polypyrrole nanowire composites are synthesized using an in situ chemical polymerization method.
- The composites effectively enhance the kinetic for the charge transfer and the ion transport.
- A remarkable specific capacitance of 696 F g^{-1} at a discharge current density of 1 A g^{-1} is observed.
- The mass ratios of graphene oxide and polypyrrole affect the electrochemical performances.

ARTICLE INFO

Article history:
Received 16 October 2012
Received in revised form
25 April 2013
Accepted 27 April 2013
Available online 8 May 2013

Keywords:
Graphene oxide
Polypyrrole nanowires
Composite
Supercapacitor

ABSTRACT

Graphene oxide/polypyrrole nanowire composite material (GO/PPy) is synthesized using an in situ chemical polymerization method. The field-emission scanning electron microscope (FE-SEM) and transmission electron microscopy (TEM) results demonstrate that the PPy nanowires with 40 nm in diameter are uniformly dispersed on the surface of GO nanosheets, which greatly increases the surface area of the material and the charge transfer reaction. This two-dimensional structure exhibits better electrochemical performance than the pure individual components. According to the galvanostatic charge/discharge analysis, the GO/PPy composite has a good supercapacitive performance with a specific capacitance of 728 F g^{-1} at a discharge current density of 0.5 A g^{-1}, higher than that of PPy nanowires (251 F g^{-1}). At a discharge current density of 2.5 A g^{-1}, the GO/PPy composite also has a high specific capacitance of 675 F g^{-1}. Significantly, the GO/PPy electrode shows excellent cycling stability (7% capacity loss after 1000 cycles) due to the GO layer releasing the intrinsic differential strain of PPy chains during long-term charge/discharge cycles.

1. Introduction

Supercapacitor, the energy storage devices between secondary batteries and traditional capacitors, has attracted considerable attention over the past decades, owing to its high power capability, short charge/discharge time, long cycle life, low self-discharging, and better environmental friendliness [1]. In supercapacitor, capacitance can arise due to reversible ion adsorption at the electrode/electrolyte interface (electrical double layer capacitors, EDLCs) or fast reversible faradic reactions at surface of electroactive materials (pseudo-capacitors) [2]. Commonly, carbon materials such as activated carbon, mesoporous carbon, and carbon nanotubes are widely used as electrode materials for EDLCs [3–5], due to their good conductivity, low cost, and long cycle life. In terms of power delivery and energy storage capacity, the crucial point for EDLCs performance is proper control over the specific surface area and micropores adapt to the size of electrolyte ions [6]. Compared with EDLCs, pseudo-capacitors employing transition metal oxides [7–9] and conducting polymers [10–12] could afford large specific capacitance. However, the application of pseudo-capacitors is usually restricted by the low working voltages, the poor stability and unsatisfactory high-rate capabilities arising from low conductivities of electrode materials [13,14].

Recent research is focused on improving the energy density of supercapacitor while maintaining its high power density. An active electrode material with high capacity performance is indispensable for developing supercapacitor device [15]. Superior performance is expected from anchoring nanostructured conducting polymers and metal oxides onto carbon materials [3,16], where the pseudo-capacitance and EDLC can function simultaneously depending on the nature of the electrode material [17]. Among the conducting polymers, carbon–polypyrrole (carbon-PPy)

* Corresponding author. Tel./fax: +86 21 50217331.
E-mail addresses: hqxie@sspu.cn, hqxie@sspu.edu.cn (H. Xie).

0378-7753/$ – see front matter © 2013 Elsevier B.V. All rights reserved.
http://dx.doi.org/10.1016/j.jpowsour.2013.04.144

composites have been extensively studied and well documented in the literature for supercapacitor applications [18,19]. The key to achieving high power and energy density supercapacitor is to explore novel electrode material with rational design of material combination [20].

Graphene, a single layer of sp^2-bonded carbon atoms, perfectly arrange into a two-dimensional honeycomb structure. The unique structure endows graphene with extraordinary physicochemical and structural properties [21,22]. Ever since the first isolation of free-standing graphene sheets in 2004 [23], this exciting new material has attracted a great deal of attention for implementing electrochemical supercapacitor applications, owing to its superb characteristics of chemical stability, good electrical conductivity, vast surface area, high flexibility, and mechanical strength [24]. However, as for graphene, the high specific capacitance and energy density are achieved by charge/discharge at low current density or cyclic voltammetry at low scan rates, which defeats the primary purpose of supercapacitor for high rate charge/discharge applications. The high restacking rate of graphene sheets is the major drawback to attain large surface area with desired electronic properties and the forecasted EDLC.

To date, various attempts have been made to exploit graphene-based electrode materials for supercapacitor applications by incorporating graphene with pseudo-capacitance materials, such as transition metal oxides and conducting polymers [20,25–28]. Graphene oxide (GO), a single sheet of graphite oxide, commonly obtained by placing graphite in a mixture of strong acids and oxidizing agents, which possesses many oxygen-containing groups on its basal planes and edges [14]. The abundant oxygen-containing groups are advantageous, which can improve the wettability of porous carbon with electrolytes [29]. Thus, GO possesses good solubility in solvents and provides fertile opportunities for constructing GO-based hybrid composites and their potential applications. Great efforts have been made to develop GO-based nanomaterials and explore their applications in biosensors [30], electronics and optoelectronics [31], drug delivery [32], enzyme immobilization [33], supercapacitors [34], and so on. However, little work has been carried out on the application of GO-based composites in supercapacitors [35–37].

In our previous work, PPy nanowires have been synthesized by in situ polymerization of pyrrole monomer in the presence of GO/cetyltrimethylammonium bromide (GO/CTAB) suspension with oxalic acid as dopant for PPy [38]. In this work, attempts have been made to attain uniform PPy nanowires coating on the surface of GO nanosheets in GO suspension using citric acid as dopant for pyrrole polymerization. A series of homogeneous composites have been explored. The supercapacitor performances of the resulting composites are tested in 1 M KCl aqueous solution. The specific capacitance of the composite can reach as high as 728 F g^{-1} at a discharge current density of 0.5 A g^{-1}, which is much larger than that of each pristine component. A combination of GO and conducting PPy nanowires may open the opportunity to prepare cheap and high performance electrode materials for supercapacitor applications.

2. Experimental

2.1. Preparation of GO nanosheets

Graphite oxide was synthesized from natural graphite using a modified Hummers method [39]. In the typical preparation, graphite (2 g) and $NaNO_3$ (1 g) were mixed with concentrated H_2SO_4 (48 mL) in a 500 mL flask. The mixture was stirred in an ice bath for 2 h. Then, $KMnO_4$ (6 g) was added slowly into the suspension. Afterward, the ice bath was removed and the reaction mixture was stirred over night at 35 °C, forming a thick paste. In the next step, 60 mL of H_2O was added into the above paste with constant agitation while the temperature was rapidly increased to 98 °C. Thereupon, the color of the solution turns from dark brown to yellow. After 6 h of vigorous stirring, the suspension was further treated with 200 mL of warm water (50 °C) and 20 mL of H_2O_2 (30%). The warm solution was washed several times with 5% HCl and water until the solution became acid free. The mixture was then filtered. The filter cake was dispersed in deionized water under ultrasonication for 10 min. Low-speed centrifugation was done at 1000 rpm for 6 min and the visible particles were removed completely from the precipitates. The small graphite oxide pieces and water soluble by-product were removed with increasing high-speed centrifugation at 8000 rpm for 20 min. The final sediment was finally redispersed in deionized water with mechanical agitation and mild sonication for 2 h at 20 °C, giving a suspension of exfoliated GO. In this process, graphite oxide was completely exfoliated down to individual sheets to form a stably dispersed GO/H_2O suspension. The concentration of the dispersion can be measured by weighing its solid content.

2.2. Synthesis of GO/PPy composites

Pyrrole was distilled under the protection of high purity N_2 and then kept in a refrigerator before use. All the other chemicals were analytical reagent and used without further purification. Before polymerization, a homogeneous GO aqueous suspension was obtained for further using. Composites of GO nanosheets and PPy nanowires with different mass ratios were synthesized using in situ polymerization of pyrrole monomer in the presence of GO suspension with different ingredient mass ratios for pyrrole and GO. The mass ratio of GO to pyrrole was varied as 1:99, 5:95, 20:80 and the resulting composites were signed as GP_{ratio}, like $GP_{1:99}$, indicating the mass ratio of GO and pyrrole was 1:99. Here we take the $GP_{5:95}$ composite as an example. 1.82 g of cetyltrimethylammonium bromide (CTAB) and 550 μL of pyrrole were added into 200 mL of exfoliated GO suspension (0.14 mg mL^{-1}) under ultrasonication for 2 h. GO nanosheets have their basal planes decorated mostly with epoxy and hydroxyl groups, while carbonyl and carboxyl groups are located at the edges. These functional groups, acting as anchor sites, enable the subsequent in situ formation of nanostructures attaching on the surfaces of GO nanosheets [40]. Because of negative charge of GO, it is expected that pyrrole molecule can be adsorbed onto the surface of GO under ultrasonication. Afterward, ammonium persulfate (APS, 0.008 mol) was dissolved in 50 mL of 0.18 M citric acid solution, and added dropwise to the above reaction system. Polymerization of pyrrole started in a few minutes, and the reaction was allowed to stir at 0–4 °C for 5 h. Finally, the resulting precipitates were filtered and washed with a large amount of water to remove any excess surfactant, and dried in a vacuum at 60 °C for 12 h. The pure PPy nanowires were also prepared by the above mentioned chemical oxidation polymerization process without the presence of GO suspension.

2.3. Characterizations

The morphology of the as-prepared samples was observed using S-4800 field-emission scanning electron microscope (FE-SEM, HITACHI). Transmission electron microscopy (TEM) was recorded with JEOL JEM-2100F electron microscope. Atomic force microscopy (AFM) image of GO nanosheets was taken on Scanning Probe Microscope SPM-9600 Series (SHIMADZU CORPORATION, Japan), with samples prepared by spin-coating GO suspension onto freshly exfoliated mica substrates.

2.4. Electrochemical measurements

Electrochemical performances were characterized by cyclic voltammetry (CV) and electrochemical impedance spectroscopy (EIS) using a CHI 660 C electrochemical analyzer system (ChenHua Instruments Co., Shanghai, China) in 1 M KCl aqueous solution, where the three-electrode system was equipped with a platinum foil counter electrode and a saturated calomel reference electrode (SCE). The electrochemical behavior was characterized within a potential window of −0.3 to 0.7 V vs. SCE. EIS was recorded in the frequency range from 10^5 to 0.1 Hz at open circuit potential with alternate current amplitude of 10 mV. Galvanostatic charge/discharge was measured using computer controlled cycling equipment (LAND, Wuhan China).

The working electrode was prepared by casting Nafion-impregnated sample onto glassy carbon electrode (GCE, Φ4 mm) surface. GCE was carefully polished with alumina powders down to 0.05 μm on a polishing cloth, rinsed thoroughly with deionized water between each polishing step, sonicated in ethanol and water, and then allowed to dry at room temperature. The mixture containing 25 mg of electroactive materials and 15 μL of Nafion (5 wt% in ethanol) was well mixed. Then, 5 mL of absolute ethanol was added to the above mixture, and ultrasonication for 1 h to obtain a homogeneous suspension. 6 μL of as-prepared suspension was dripped onto the GCE surface and dried at room temperature before the electrochemical test. The loading amount of electroactive materials and thickness of the film can be controlled based on the amount of the dripping suspension. For comparison, the supercapacitor electrodes were also prepared by mixing 85 wt% electroactive materials with 10 wt% acetylene black as a conductive agent and 5 wt% polytetrafluoroethylene (PTFE) dissolved in ethanol as a binder to form slurry. The resulting mixture was coated onto the nickel foam substrate (1 × 1 cm^2), and then pressing and drying under vacuum at 100 °C for 12 h.

3. Results and discussion

3.1. Microstructure characterizations

AFM was applied to determine the as-synthesized GO nanosheets. An AFM image is shown in Fig. 1 with the height profile. The thickness of GO is about 0.8 nm, implying GO sheets existed in water with exfoliated structure.

The surface morphologies of PPy and GO/PPy composites can be investigated and observed from the TEM images, as shown in Fig. 2. Fig. 2a shows that pure PPy nanowires have been synthesized with hundreds of nanometers in length and 40 nm in width. The composites of $GP_{1:99}$, $GP_{5:95}$ and $GP_{20:80}$ with a similar nanostructure aggregate together (Fig. 2b–d), from which we can see that the thin layers of PPy nanowires with diameter of 40 nm are coated on the surface of GO nanosheets. While using oxalic acid as dopant for PPy polymerization, the PPy nanowires with diameter of 60 nm are attached on the surface of GO nanosheets [38]. The GO/PPy composites are formed owing to the strong π–π stacking interaction between the monolayer of GO and the electronic structures of the conjugated backbones of PPy. GO bring negative charge because of its abundant oxygen-containing functional groups. Therefore, it is expected that pyrrole molecules can be adsorbed to the surface of GO nanosheets under ultrasonication. With the addition of APS, the pyrrole monomers are initiated to polymerize just from the absorbed sites and coated onto the surface of GO nanosheets.

FE-SEM characterization was also used to investigate the structure and morphology of the samples, as shown in Fig. 3. The pure PPy showed nanowire morphology with a diameter of about 40 nm (Fig. 3a). The result was similar to the TEM image shown. As

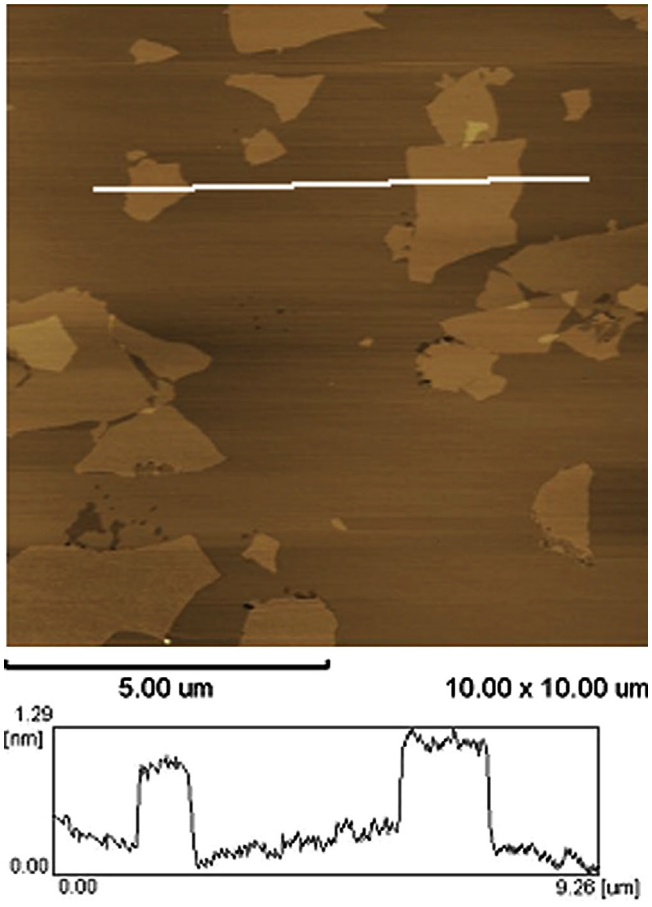

Fig. 1. AFM analysis of GO nanosheets on mica surface with height profile.

to $GP_{1:99}$, the PPy was formed and fixed to the surface of GO nanosheets after chemical polymerization (Fig. 3b). The oxygen-containing functional groups on GO sheets acted as active sites and enabled the in situ polymerization of PPy. Because of the nanofibrillar morphology and high overall coverage of PPy, the GO sheets cannot be observed clearly. Compared to $GP_{1:99}$, the amount of PPy nanowires decreased and was distributed regularly on the surface of the $GP_{5:95}$ (Fig. 3c). PPy nanowires with a diameter of 40 nm were also observed in the composite of $GP_{20:80}$ (Fig. 3d). From Fig. 3d, GO nanosheets can be clearly seen because of increasing amount of GO nanosheets in $GP_{20:80}$. Increasing the volume of pyrrole resulted in more PPy nanowires (like $GP_{1:99}$). The composite structure provided a larger surface area for the electrochemical reaction, which indicated superior electrochemical performance.

3.2. Electrochemical behavior

The electrochemical performances of supercapacitor were evaluated by using CV, galvanostatic charge/discharge and EIS techniques. The specific capacitance of the electrode can be calculated according to the following equation from CV curves:

$$C = \left(\int I dV\right) \Big/ (vmV) \quad (1)$$

where C is the specific capacitance based on the mass of electroactive materials (F g^{-1}), I is the response current (A), V is the potential (V), v is the potential scan rate (V s^{-1}), and m is the mass of the electroactive materials (g).

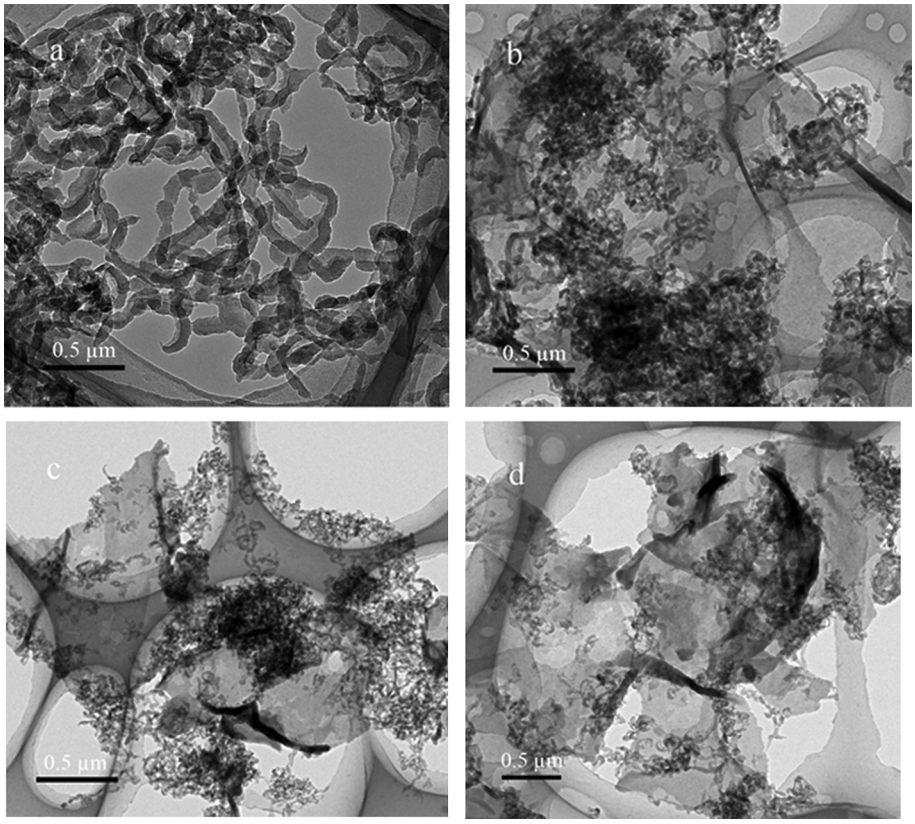

Fig. 2. TEM images of PPy and GO/PPy composites. (a) PPy, (b) $GP_{1:99}$, (c) $GP_{5:95}$ and (d) $GP_{20:80}$.

The supercapacitor electrode material was first characterized by CV measurements against SCE with a potential range between −0.3 and 0.7 V at different scan rates in 1 M KCl, as shown in Fig. 4. All CV curves maintain rectangular shape with only small distortions even at a high scan rate, indicative of highly capacitive nature with good ion response. The large surface areas and ultrathin PPy nanowires not only provide more electrochemically active sites but also shorten the distance for ion and electron transportation. The CV curves at a scan rate of 300 mV s^{-1} are not rectangular and opened at the low-voltage side due to polarization of the electrodes. At high

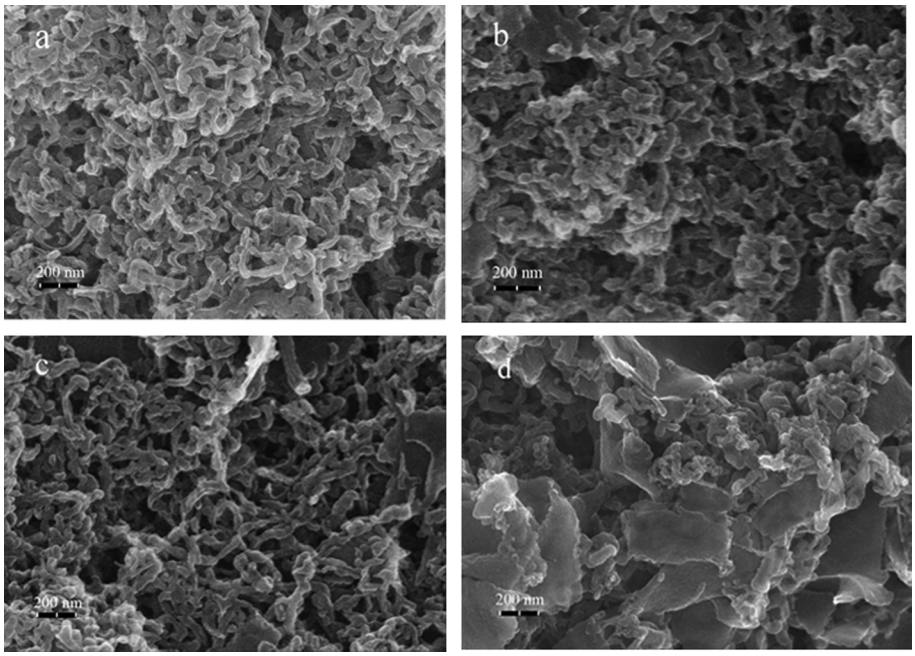

Fig. 3. FE-SEM images of the GO/PPy composites. (a) PPy, (b) $GP_{1:99}$, (c) $GP_{5:95}$ and (d) $GP_{20:80}$.

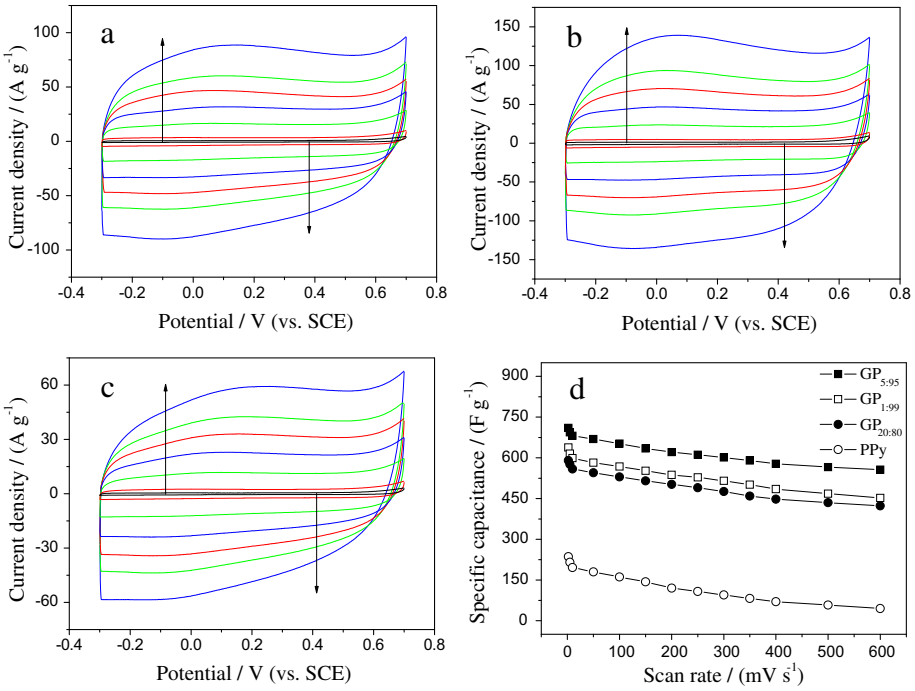

Fig. 4. CV curves of the GO/PPy composites at different scan rates of 2, 10, 50, 100, 150, 200 and 300 mV s^{-1}. (a) $GP_{1:99}$, (b) $GP_{5:95}$ and (c) $GP_{20:80}$. (d) The variation of the specific capacitance of PPy nanowires and the GO/PPy composites at different scan rates.

scan rate, the concentration of ions on the solid/liquid interface increase rapidly and the diffusion rate of electrolyte from solid/liquid interface to electrode material is not fast enough to satisfy the electrochemical reactions of electrode materials. These results in the enrichment of electrolyte near the solid/liquid interface and polarization of the electrode materials [27]. The variations of specific capacitance as a function of scan rates are plotted in Fig. 4d. The specific capacitances are 638, 710, 590 and 236 F g^{-1} for samples of $GP_{1:99}$, $GP_{5:95}$, $GP_{20:80}$ and pure PPy at 2 mV s^{-1}, respectively. The specific capacitance of GO is 52 F g^{-1}. By further increasing the scan rate to 600 mV s^{-1}, the specific capacitances are still as high as 452, 556, 423 and 45 F g^{-1} for these samples, which indicates that the composites have good rate capability.

The electroactive materials of $GP_{1:99}$, $GP_{5:95}$ and $GP_{20:80}$ coated onto the nickel foam substrate were also investigated by CV measurements in a potential window of −0.3 to 0.7 V vs. SCE in 1 M KCl aqueous solution at a scan rate of 2 mV s^{-1}, as illustrated in Fig. 5 (curve d–f). Each electrode contained 12 mg of electroactive material. For a comparison, the CV curves of supercapacitor electrodes fabricated using the GCE substrate were also presented in Fig. 5 (curve a–c). It can be seen all CV curves exhibit an approximately rectangular shape. It is apparently found that the surrounded by CV curves of $GP_{5:95}$ coated on the GCE substrate (curve b) is apparently largest, indicating highest specific capacitance. The specific capacitances of $GP_{1:99}$, $GP_{5:95}$ and $GP_{20:80}$ coated on the nickel foam substrate are 621, 695 and 582 F g^{-1} at a scan rate of 2 mV s^{-1}, respectively. Besides, the capacitive performances of GO/PPy composites on the GCE are enhanced to different degrees as the mass ratio changes, which can be ascribed to good electrical conductivity of the GCE substrate and a small amount of electroactive material.

The GO/PPy composites have superior electrochemical performance than that of pure PPy nanowires and GO electrode. Although GO is not able to directly serve as an electrode material due to its poor conductivity, the hydrophilic GO can offer high coverage available for the double-layer formation and charge-transfer reaction, and then improve the electrochemical performance of the composite. Thus, the obtained GO/PPy composites exhibit large specific capacitance owing to their synergistic performance as electrode material. As to GO/PPy composite, $GP_{5:95}$ has relatively excellent electrochemical properties compared with $GP_{1:99}$ and $GP_{20:80}$. It can be attributed to the fact that the extra formed PPy nanowires are not closely combined with GO nanosheets in the composite of $GP_{1:99}$, which would decrease the electron transportation, leading to a lower contribution to the specific capacitance of the composite. With increasing the content of GO in the composite, the specific capacitance has obvious enhancement ($GP_{5:95}$), assigned to the intimate interaction of both components facilitate the electron transport from PPy to the underlying GO

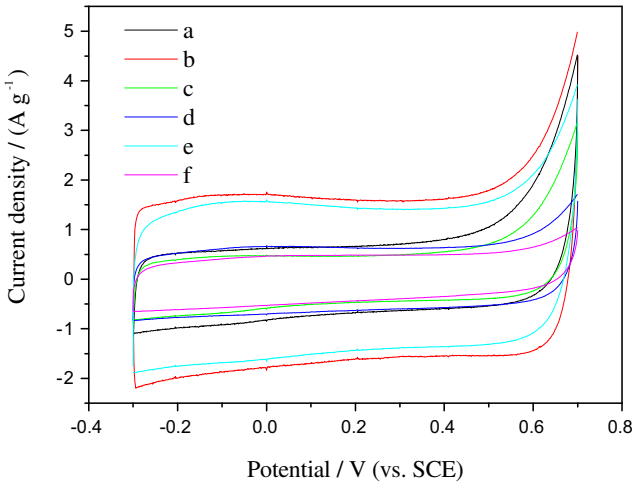

Fig. 5. CV curves of the GO/PPy composites coated onto the GCE (a–c) and nickel foam substrate (d–f) at a scan rate of 2 mV s^{-1}. (a and d) $GP_{1:99}$, (b and e) $GP_{5:95}$, and (c and f) $GP_{20:80}$. The electroactive materials on the GCE are 30 μg and 12 mg on the nickel foam substrate.

nanosheets, leading to rapid redox reactions. However, the specific capacitance of $GP_{20:80}$ decreases, which may be attributed to the larger fraction of GO would affect the growth of PPy nanowires. These results mean that introducing less content of GO into PPy matrix can effectively increase the capacitive performance, resulting in the high electrochemical utilization of PPy and GO nanosheets.

The specific capacitance and rate capability of the supercapacitor are also revealed by galvanostatic measurements. The galvanostatic charge/discharge curves of PPy, $GP_{1:99}$, $GP_{5:95}$ and $GP_{20:80}$ electrodes at current densities of 1 A g^{-1} and 2.5 A g^{-1} are shown in Fig. 6. The charge/discharge curves of $GP_{1:99}$, $GP_{5:95}$ and $GP_{20:80}$ almost maintain the similar shape in the potential range from −0.3 to 0.7 V at the same current density, revealing that the hybrid electrode material can experience a broad electric current range. Based on the charge/discharge curve, the specific capacitance can be calculated according to the following equation:

$$C_m = I \times \Delta t/(\Delta V \times m) \quad (2)$$

where I is the discharge current (A), Δt is the discharge time (s), ΔV is the voltage change during the discharge process (V), and m is the mass of electroactive material (g). The specific capacitances of electrodes are summarized in Fig. 6c. The specific capacitance of $GP_{5:95}$ is higher than that of $GP_{1:99}$, $GP_{20:80}$ and pure PPy under the same discharge current density, which can be clearly found from the specific capacitance curves. The specific capacitances of $GP_{1:99}$, $GP_{5:95}$, $GP_{20:80}$ and PPy electrodes at a discharge current density of 0.5 A g^{-1} are 661, 728, 605 and 251 F g^{-1}, respectively. At a current density of 1 A g^{-1}, the specific capacitance of $GP_{5:95}$ is 696 F g^{-1}, which is higher than GO/PPy composite with oxalic acid as dopant [38]. Even at a high current density of 8 A g^{-1}, the specific capacitance of $GP_{5:95}$ remains 601 F g^{-1}, while that of pure PPy sharply decreases to 80 F g^{-1}. $GP_{1:99}$ and $GP_{20:80}$ exhibit specific capacitance of about 503 and 469 F g^{-1} at a discharge current density of 8 A g^{-1}. It is noted that the $GP_{5:95}$ show not only high capacitance but also better rate capability, indicating this ratio is optimal among all the samples. The improved specific capacitance and better rate capability of $GP_{5:95}$ might be mainly ascribed to the synergetic effect between the two components, which can shorten ion diffusion length and make higher materials utilization. The electroactive materials coated onto the nickel foam substrate were also investigated by galvanostatic charge/discharge measurements. The specific capacitances of $GP_{1:99}$, $GP_{5:95}$ and $GP_{20:80}$ electrodes at a discharge current density of 1 A g^{-1} are 598, 681 and 567 F g^{-1}, respectively.

Electrochemical impedance tests were carried out to evaluate the charge transfer and electrolyte diffusion in the electrode/electrolyte interface, as shown in Fig. 7. It is notable that pure PPy electrode presents well-defined semicircle over the high-frequency range, followed by a straight sloped line in the low-frequency region. The Nyquist plots of $GP_{5:95}$ and GO electrodes show small semicircle regions and short Warburg regions. In the semicircle regions, the two electrodes exhibit the similar characteristic frequencies as high as 4.5 kHz, reflecting the rapid charge transfer process in both electrodes. The Warburg regions of both electrodes are also the same (from 97.8 to 3.1 Hz), which demonstrate the fast electrolyte diffusions in the electrodes. The $GP_{5:95}$ electrode exhibits a more vertical line than PPy and GO electrodes at low-frequency, illustrating better capacitive behavior and lower diffusion resistance of ions. In the high frequency region, the intersection of the semicircle with the real axis represents the resistance of the electrolyte solution (R_s). The intercept of $GP_{5:95}$ (0.17 Ω) is much smaller than that of PPy (0.9 Ω) and GO (0.24 Ω). The hydrophilic GO can provide enhanced electrode/electrolyte interface areas, which enable the electrochemical accessibility of electrolyte through the loosely packed PPy nanowires structure, facilitating rapid transport of the electrolyte ions in the electrode during charge/discharge processes. Therefore, the composites can greatly reduce the diffusion length, resulting in the improvement of electrochemical properties of GO/PPy composite materials.

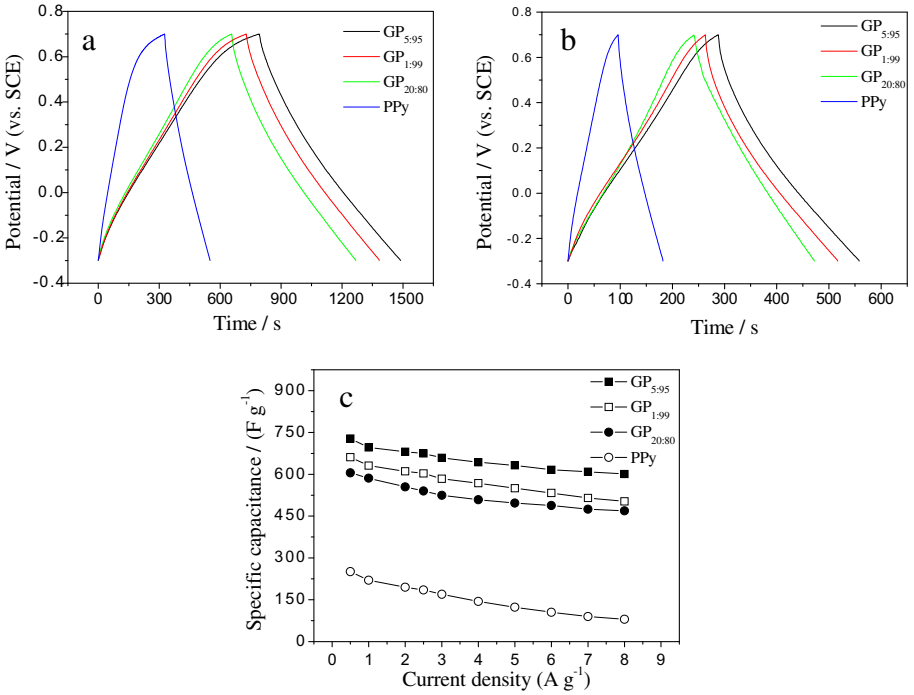

Fig. 6. Galvanostatic charge/discharge curves of $GP_{1:99}$, $GP_{5:95}$, $GP_{20:80}$, and PPy at current densities of (a) 1 A g^{-1} and (b) 2.5 A g^{-1}. (c) The specific capacitances of these electrodes at different current densities. The mass of sample is 30 μg.

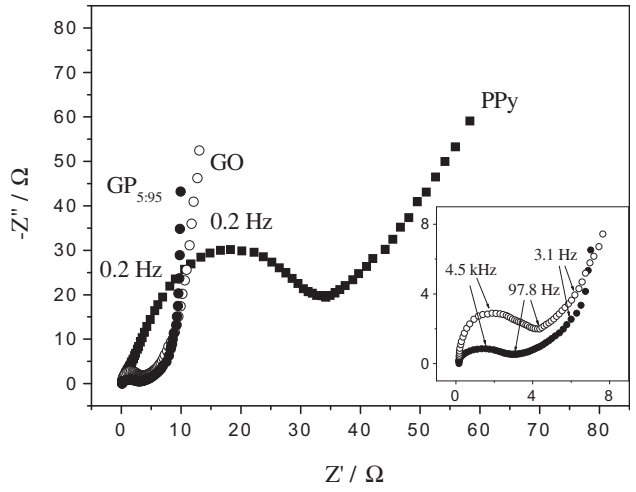

Fig. 7. Impedance spectra of pure PPy, GO and the composite of $GP_{5:95}$ in 1 M KCl solution measured at open circuit potential.

Long cycle life is a crucial parameter for supercapacitor electrode materials. The electrochemical stabilities of pure PPy and $GP_{5:95}$ were investigated by repeating the CV test between −0.3 and 0.7 V at a scan rate of 50 mV s^{-1} for 1000 cycles. The specific capacitance of the electrode materials as a function of cycle number is presented in Fig. 8. The inset illustrates the changes of CV curves at the 1st and 1000th cycles. The specific capacitance of the $GP_{5:95}$ decreases in the first 100 cycles and thereafter an increase for the 100–400 cycles. The increase of the specific capacitance is may be due to that the oxygen groups on the GO are further reduced by electrochemical reaction, which is consistent with other report [41]. Besides, the activation of electrode material also leads to higher conductivity because of better contact between electrolyte and electrode material. Then, the specific capacitance maintain approximately steady, indicating the electrode is fully activated and reach the optimum condition. After 1000 cycles, the $GP_{5:95}$ electrode exhibits capacitive retentions of about 93%, while just only 60% for PPy. The conducting polymers may cause swelling and shrinkage in charge/discharge process, which may lead to degradation of the polymeric conductivity and charge storage capability [42]. The best method to alleviate this limitation is the combination

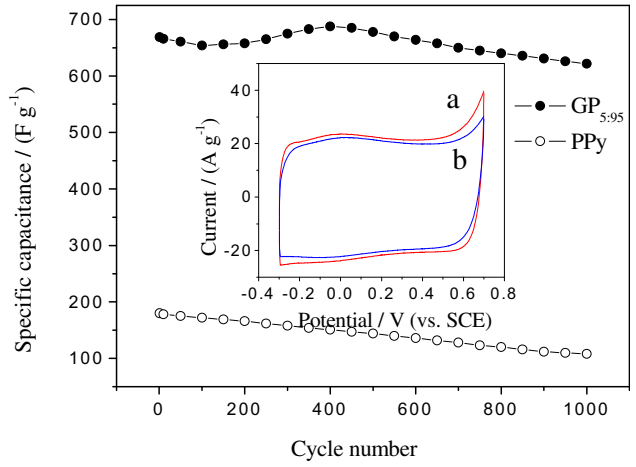

Fig. 8. Cycle life of PPy and $GP_{5:95}$ composite electrodes at 50 mV s^{-1} in 1 M KCl solution. Inset shows the CV curves of the 1st (curve a) and 1000th (curve b) cycles of the $GP_{5:95}$.

of conducting polymers with carbon materials, which has been proved to reinforce the stability of conducting polymers as well as maximize the capacitance value [43,44]. In GO/PPy composite, GO nanosheets can act as the frameworks for sustaining PPy nanowires, preventing PPy chains from severely swelling and shrinking during charge/discharge process. The GO layered structure would also avoid the destruction of the electrode material and is beneficial for a better stability during the charge/discharge processes.

The reproducibility of electrochemical capacitances of $GP_{1:99}$, $GP_{5:95}$ and $GP_{20:80}$ composites are also tested by repetitive recording of CVs in 1 M KCl solution. It is found that the relative standard deviation (R.S.D.) of the specific capacitance for 20 replicate determinations is 3.2%, 2.9 and 3.6%, respectively. Ten pieces of the proposed supercapacitor electrodes are fabricated and the R.S.D. for the individual determination is 3.4%, 3.1% and 3.3%, respectively. These results demonstrate that fabricated supercapacitor electrodes have excellent reproducibility. Based on the specific microstructures and intrinsic electrochemical properties, the GO/PPy composites can be applied as electrode materials for electrochemical supercapacitors.

4. Conclusions

Composite of GO and PPy nanowires was prepared using a simple in situ chemical oxidation polymerization procedure. The PPy nanowires with diameter of 40 nm can be synthesized on GO nanosheet surface. Supercapacitors based on the GO/PPy composites exhibited high specific capacitance, good rate capability and cycling stability. The nanowires of PPy was induced and greatly affected by the addition of GO in the synthesized process, which might greatly contribute to the electrochemical properties of the composite. With a small content of GO ($GP_{5:95}$) in the composite, not only the specific capacitance but also its rate capability is enhanced. The $GP_{5:95}$ electrode showed specific capacitance as high as 728 and 675 F g^{-1} at a discharge current density of 0.5 and 2.5 A g^{-1}, respectively. The specific capacitance retained 93% of the initial capacitance after 1000 cycles at a scan rate of 50 mV s^{-1}, suggesting superior electrochemical rate capability and cycling stability. These results afforded an easy and efficient way to construct GO/PPy composites for the increasing demands on the high performance energy storage devices. Further optimization and control of the structures to exploit better electrochemical properties of graphene and PPy composites are under investigation in our group.

Acknowledgments

This work was supported by the Shanghai Municipal Education Commission, Shanghai Educational Development Foundation (11CG64), the Innovation Program of Shanghai Municipal Education Commission (12YZ179, 13ZZ139), the National Science Foundation of China (51176106), Fundamental and Priority Program of Shanghai Committee of Science and Technology (12JC1404300), the Program for New Century Excellent Talents in University (NCET-10-883) and the Program for Professor of Special Appointment (Eastern Scholar) at Shanghai Institutions of Higher Learning.

References

[1] L.L. Zhang, R. Zhou, X.S. Zhao, J. Mater. Chem. 20 (2010) 5983–5992.
[2] B.E. Conway, Electrochemical Supercapacitors: Scientific Fundamentals and Technological Applications, Kluwer Academic/Plenum Press, New York, 1999.
[3] H.Q. Wang, Z.S. Li, Y.G. Huang, Q.Y. Li, X.Y. Wang, J. Mater. Chem. 20 (2010) 3883–3889.
[4] H.J. Liu, X.M. Wang, W.J. Cui, Y.Q. Dou, D.Y. Zhao, Y.Y. Xia, J. Mater. Chem. 20 (2010) 4223–4230.

[5] R.F. Zhou, C.Z. Meng, F. Zhu, Q.Q. Li, C.H. Liu, S.S. Fan, K.L. Jiang, Nanotechnology 21 (2010) 345701, 7p.
[6] C. Largeot, C. Portet, J. Chmiola, P.L. Taberna, Y. Gogotsi, P. Simon, J. Am. Chem. Soc. 130 (2008) 2730–2731.
[7] F. Ataherian, N.L. Wu, J. Electrochem. Soc. 158 (2011) A422–A427.
[8] H. Xia, J.K. Feng, H.L. Wang, M.O. Lai, L. Lu, J. Power Sources 195 (2010) 4410–4413.
[9] J.H. Kim, D.S. Kil, S.J. Yeom, J.S. Roh, N.J. Kwak, J.W. Kim, Appl. Phys. Lett. 91 (2007).
[10] G.Y. Zhao, H.L. Li, Microporous Mesoporous Mater. 110 (2008) 590–594.
[11] H.Y. Mi, X.G. Zhang, X.G. Ye, S.D. Yang, J. Power Sources 176 (2008) 403–409.
[12] W. Sun, R.L. Zheng, X.Y. Chen, J. Power Sources 195 (2010) 7120–7125.
[13] R. Liu, S.B. Lee, J. Am. Chem. Soc. 130 (2008) 2942–2943.
[14] Y.Q. Sun, Q.O. Wu, G.Q. Shi, Energy Environ. Sci. 4 (2011) 1113–1132.
[15] J. Yan, T. Wei, B. Shao, Z.J. Fan, W.Z. Qian, M.L. Zhang, F. Wei, Carbon 48 (2010) 487–493.
[16] L.X. Li, H.H. Song, Q.C. Zhang, J.Y. Yao, X.H. Chen, J. Power Sources 187 (2009) 268–274.
[17] P. Simon, Y. Gogotsi, Nat. Mater. 7 (2008) 845–854.
[18] Y.P. Fang, J.W. Liu, D.J. Yu, J.P. Wicksted, K. Kalkan, C.O. Topal, B.N. Flanders, J.D. Wu, J. Li, J. Power Sources 195 (2010) 674–679.
[19] H.F. An, Y. Wang, X.Y. Wang, L.P. Zheng, X.Y. Wang, L.H. Yi, L. Bai, X.Y. Zhang, J. Power Sources 195 (2010) 6964–6969.
[20] G.H. Yu, L.B. Hu, M. Vosgueritchian, H.L. Wang, X. Xie, J.R. McDonough, X. Cui, Y. Cui, Z.N. Bao, Nano Lett. 11 (2011) 2905–2911.
[21] D.S.L. Abergel, V. Apalkov, J. Berashevich, K. Ziegler, T. Chakraborty, Adv. Phys. 59 (2010) 261–482.
[22] M.J. Allen, V.C. Tung, R.B. Kaner, Chem. Rev. 110 (2010) 132–145.
[23] K.S. Novoselov, A.K. Geim, S.V. Morozov, D. Jiang, Y. Zhang, S.V. Dubonos, I.V. Grigorieva, A.A. Firsov, Science 306 (2004) 666–669.
[24] C.N.R. Rao, A.K. Sood, K.S. Subrahmanyam, A. Govindaraj, Angew. Chem. Int. Ed. 48 (2009) 7752–7777.
[25] R.L. Liang, H.Q. Cao, D. Qian, J.X. Zhang, M.Z. Qu, J. Mater. Chem. 21 (2011) 17654–17657.
[26] Q.L. Hao, H.L. Wang, X.J. Yang, L.D. Lu, X. Wang, Nano Res. 4 (2011) 323–333.
[27] J. Sun, C.H. Xu, L. Gao, J. Mater. Chem. 21 (2011) 11253–11258.
[28] B. Zhao, J.S. Song, P. Liu, W.W. Xu, T. Fang, Z. Jiao, H.J. Zhang, Y. Jiang, J. Mater. Chem. 21 (2011) 18792–18798.
[29] C.T. Hsieh, W.Y. Chen, Y.S. Cheng, Electrochim. Acta 55 (2010) 5294–5300.
[30] J.H. Jung, D.S. Cheon, F. Liu, K.B. Lee, T.S. Seo, Angew. Chem. Int. Ed. 49 (2010) 5708–5711.
[31] G. Eda, M. Chhowalla, Adv. Mater. 22 (2010) 2392–2415.
[32] X.M. Sun, Z. Liu, K. Welsher, J.T. Robinson, A. Goodwin, S. Zaric, H.J. Dai, Nano Res. 1 (2008) 203–212.
[33] J.L. Zhang, F. Zhang, H.J. Yang, X.L. Huang, H. Liu, J.Y. Zhang, S.W. Guo, Langmuir 26 (2010) 6083–6085.
[34] B. Xu, S.F. Yue, Z.Y. Sui, X.T. Zhang, S.S. Hou, G.P. Cao, Y.S. Yang, Energy Environ. Sci. 4 (2011) 2826–2830.
[35] C.Z. Zhu, J.F. Zhai, D. Wen, S.J. Dong, J. Mater. Chem. 22 (2012) 6300–6306.
[36] J.J. Xu, K. Wang, S.Z. Zu, B.H. Han, Z.X. Wei, ACS Nano 4 (2010) 5019–5026.
[37] S. Chen, J.W. Zhu, X.D. Wu, Q.F. Han, X. Wang, ACS Nano 4 (2010) 2822–2830.
[38] J. Li, H.Q. Xie, Mater. Lett. 78 (2012) 106–109.
[39] W.S. Hummers, R.E. Offeman, J. Am. Chem. Soc. 80 (1958), 1339–1339.
[40] C. Xu, X. Wang, J. Zhu, X. Yang, L. Lu, J. Mater. Chem. 18 (2008) 5625–5629.
[41] Y.Y. Shao, J. Wang, M. Engelhard, C.M. Wang, Y.H. Lin, J. Mater. Chem. 20 (2010) 743–748.
[42] V. Khomenko, E. Frackowiak, F. Beguin, Electrochim. Acta 50 (2005) 2499–2506.
[43] H. Tamai, M. Hakoda, T. Shiono, H. Yasuda, J. Mater. Sci. 42 (2007) 1293–1298.
[44] H.Y. Mi, X.G. Zhang, S.Y. An, X.G. Ye, S.D. Yang, Electrochem. Commun. 9 (2007) 2859–2862.